Faraday Discussions

Cite this: *Faraday Discuss.*, 2014, **176**, 251

PAPER

Mesoscopic photosystems for solar light harvesting and conversion: facile and reversible transformation of metal-halide perovskites

Hauke Arne Harms,[a] Nicolas Tétreault,[a] Norman Pellet,[a] Michaël Bensimon[b] and Michael Grätzel*[a]

Received 20th August 2014, Accepted 2nd September 2014
DOI: 10.1039/c4fd00160e

Recently, hybrid organic–inorganic metal halide perovskites have gained prominence as potent light harvesters in thin film solid-state photovoltaics. In particular the solar-to-electric power conversion efficiency (PCE) of devices using $CH_3NH_3PbI_3$ as sensitizer has increased from 3 to 20.1% within only a few years. This key material can be prepared by solution processing from PbI_2 and CH_3NH_3I in one step or by sequential deposition. In the latter case an electron capturing support such as TiO_2 is first covered with PbI_2, which upon exposure to a CH_3NH_3I solution is converted to the perovskite. Here we apply for the first time quartz crystal microbalance (QCMD) measurements in conjunction with X-ray diffraction and scanning electron microscopy to analyse the dynamics of the conversion of PbI_2 to $CH_3NH_3PbI_3$. Employing 200 nm thick PbI_2 films as substrates we discover that the CH_3NH_3I insertion in the PbI_2 is reversible, with the extraction into the solvent isopropanol occurring on the same time scale of seconds as the intercalation process. This offers an explanation for the strikingly rapid and facile exchange of halide ions in $CH_3NH_3PbX_3$ by solution processing at room temperature.

1 Introduction

The application of hybrid organic–inorganic methylammonium metal halide perovskites in photovoltaic cells has gained importance over the last few years, mainly due to the surge in published power conversion efficiency from 3.8% in 2009 up to 20.1% certified efficiency in 2014.[1–8] The concept of using a perovskite material in the device architecture of a solid-state dye sensitized solar cell can be seen as a result of the search for inorganic absorber materials other than quantum dots or Sb_2S_3, that can fulfil a similar function as the molecular

[a]*Laboratory for Photonics and Interfaces (LPI), Faculty of Basic Science, EPFL, Lausanne, Switzerland. E-mail: michael.graetzel@epfl.ch; Fax: +41 (0)21 6936100; Tel: +41 (0)21 6933112*

[b]*Central Environmental Laboratory (CEL), Environmental Engineering Institute (IIE), EPFL, Lausanne, Switzerland. E-mail: michael.bensimon@epfl.ch; Fax: +41 (0)21 6936330; Tel: +41 (0)21 6932331*

absorber in a dye sensitized solar cell. Methylammonium lead iodide has proven the most successful material yet, and size estimations of the constituting lattice by Mashiyama *et al.* as well as by Mitzi *et al.* suggest that it forms more stable crystals than other methylammonium lead halides.[9] Methylammonium tin halide perovskites are less stable than their lead counterparts due to the facile oxidation of Sn^{2+} to Sn^{4+}.

One route to high-efficiency devices employs a sequential deposition of a PbI_2 film that is subsequently converted to $CH_3NH_3PbI_3$ perovskite by incorporation of methylammonium iodide (CH_3NH_3I or MAI) from solution. This route, which often gives better morphological control over the resulting film than a one-step deposition of the perovskite, was first successfully demonstrated on a mesoporous titania film by Burschka *et al.*,[6] attaining efficiencies of 15% and more recently over 17% [J.-H. Im, I.-H. Jang, N. Pellet,[2] M. Grätzel and N. G. Park, *Nat. Nanotechnol.*, 2014, **9** (11), 927–932].

The sequential deposition has been adapted to the conversion of PbI_2 films on compact titania and zinc oxide films, which are solution-processed at low temperatures and yield power conversion efficiencies of 13.7% and 15.7%, respectively.[10,11]

1.1 Perovskite structure

Fig. 1 illustrates the crystal structure of the ideal perovskite. The ideal ABX_3 compound crystallises in a cubic unit cell with the larger cation A in its centre, and the smaller cation B located at the corners. The smaller cation B is octahedrally coordinated to the anions X that lie at the centre of the edges of the cubic unit cell. In inorganic–organic hybrid perovskites, there is often a competition between the 3-dimensional perovskite structure ABX_3, and the 2-dimensional perovskite structure A_2BX_4 because of the size difference between the organic cation A and the inorganic cation B. The 2-dimensional perovskite consists of corner-sharing BX_6 octahedra that are separated by a double layer of organic cations A. This layered structure does in principle impose no limitations on the size of the organic cation A.

The synthesis of phase-pure organic–inorganic hybrid perovskites can be difficult, and methylammonium along with formamidinium is one of the few organic cations that readily crystallises in a 3-dimensional perovskite structure

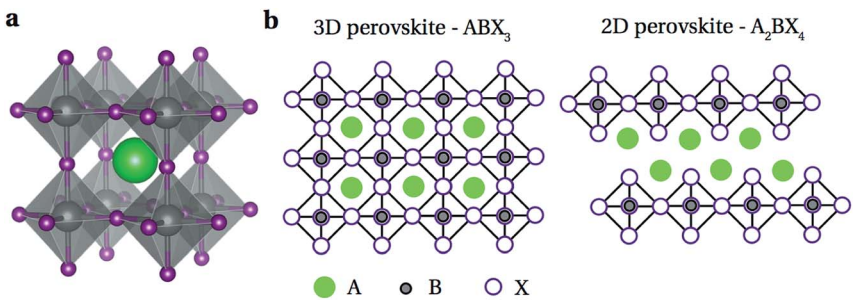

Fig. 1 A perspective view of the perovskite ABX_3 crystal structure is shown in part (a). Projected views of the 3-dimensional ABX_3 perovskite and the 2-dimensional A_2BX_4 perovskite crystal structure are given in (b). Graphic from Burschka.[12]

when used in a lead-halide or tin-halide compound. Methylammonium tin halide perovskites are less stable than their lead counterparts because of the facile oxidation of Sn^{2+} to Sn^{4+}. Regarding the different methylammonium lead-halide perovskites, the iodide compound $CH_3NH_3PbI_3$ has attracted the most interest for photovoltaic applications due its strong light absorption covering all the visible range.

1.2 Methylammonium lead iodide perovskites for photovoltaic applications and their synthesis by conversion from lead-iodide salt

The direct bandgap of $CH_3NH_3PbI_3$ is 1.54 eV which corresponds to an absorption onset at approximately 800 nm. In a typical solar cell configuration, the perovskite absorber is contacted by TiO_2 on one side, acting as an electron-selective contact and as an n-type conductor. The other side of the perovskite is contacted with a hole transport material acting as a hole-selective contact, usually spiro-MeOTAD (2,2′,7,7′-tetrakis(*N*,*N*-di-*para*-methoxyphenyl-amine)-9-9′-spiro-bifluorene). Fig. 2 shows a simplified energy level diagram for this configuration on a scale against vacuum. The valence band of the $CH_3NH_3PbI_3$ was measured to be −5.4 eV by ultraviolet photoelectron spectroscopy.[3] Considering the optical bandgap of 1.54 eV, the conduction band edge lies around −3.9 eV. If we use the published value of −4.0 eV for the TiO_2 conduction band, and of −5.1 eV for the valence band of spiro-MeOTAD, we obtain an offset of 0.1 eV between the conduction bands of the perovskite and the TiO_2, and 0.3 eV between the valence band of the perovskite and the spiro-MeOTAD. The valence band and conduction band of the $CH_3NH_3PbI_3$ perovskite are formed only by the orbitals of Pb and I, whereas the organic cation has no direct contribution. However the size of the organic cation influences the structure of the perovskite crystal and thereby the overlap between the orbitals of Pb and I, affecting its optoelectronic properties.

The crystal phase of $CH_3NH_3PbI_3$ depends on temperature, and three different phases have been observed.[13] The ideal cubic perovskite phase prevails at temperatures above 54 °C, and allows for rapid reorientation of the methylammonium cation that can occupy 24 different disordered states.[14] Between 54 °C

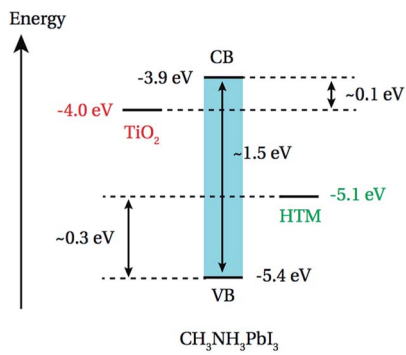

Fig. 2 Simplified energy diagram, illustrating the conduction and valence band of the perovskite as well as the conduction band of TiO_2 and the valence band of the hole transport material spiro-MeOTAD. All energy levels are given in eV against vacuum level. Graphic from Burschka.[12]

and −112 °C, the PbI_2 octahedra undergo a tilting around the *c*-axis of the crystal and thereby reduce the structure to a tetragonal phase, limiting the number of disordered states of the methylammonium cation to 8 possibilities. Below −112 °C, the $CH_3NH_3PbI_3$ crystallises in an orthorhombic phase, and the alignment of the methylammonium anion is fixed. For the $CH_3NH_3PbI_3$ material, no 2-dimensional phase of the form A_2BX_4 has been observed.

For a single-step deposition methods, the perovskite is usually processed by dissolving two precursors, CH_3NH_3I and PbI_2, in polar organic solvents like γ-butyrolactone or *N*,*N*-dimethylformamide (DMF). The $CH_3NH_3PbI_3$ perovskite readily crystallises at room temperature upon evaporation of the solvent. However, it can be difficult to control the film morphology or the infiltration of mesoporous films when crystallising the perovskite material directly from solution. In order to achieve a better control of film morphology, Burschka *et al.* further developed a previously described method of sequential deposition.[6,17] First, a PbI_2 film is deposited by spin-casting a concentrated PbI_2 solution in DMF which subsequently is exposed to a solution of methylammonium iodide in a solvent such as isopropanol that does not dissolve the PbI_2. The process is illustrated in Fig. 3.

Two-step-depositions which entail a conversion reaction are often used to achieve a certain morphology. One example from literature is the conversion of II–V semiconductor nanostructures to III–V materials by ion exchange reactions whilst maintaining the initial architecture.[17] In those examples, the thermodynamic driving force was the difference in bulk lattice energy between the different compounds. Here, the starting material PbI_2 is itself a well-studied semiconductor. PbI_2 crystallises in layers of edge-sharing PbI_6 octahedra, which lead to strong intralayer bonding in a hexagonal crystal lattice, but only weak interlayer bonding, which allows for the formation of different polytypes for the stacking of layers. Fig. 4 is an illustration of the crystal structure of PbI_2 in the most prevalent layer stacking of the 2H polytype. The weak interlayer bonding seems to allow for rapid intercalation of guest molecules into the PbI_2 crystal. The conversion results into a two-fold increase of volume per formula, as can be estimated from the lattice parameters for PbI_2 and $CH_3NH_3PbI_3$ that are listed in Table 1. The

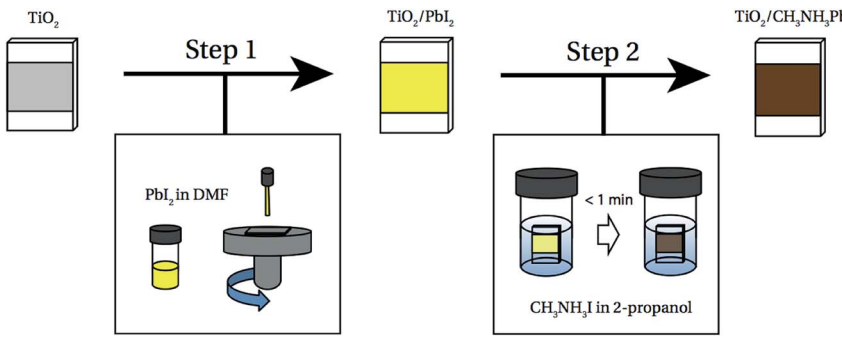

Fig. 3 Schematic illustration of the sequential deposition technique in two steps. First, a PbI_2 film is spin-cast from a solution of DMF. Subsequently, the film is immersed in a solution of CH_3NH_3I in isopropanol for less than one minute. In our experimental work, a pre-wetting with isopropanol has been applied prior to the second step. From Burschka.[12]

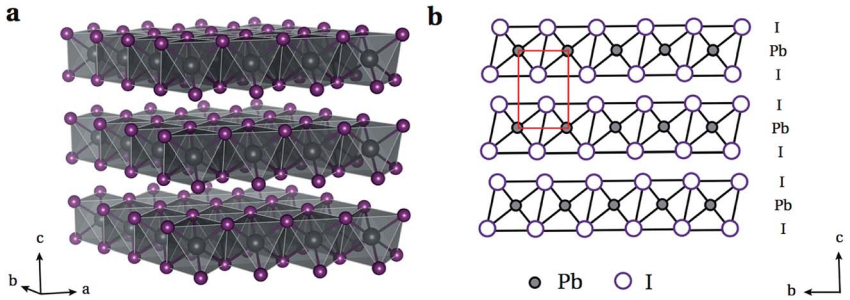

Fig. 4 Illustration of the layered PbI_2 crystal structure in the hexagonal 2H polytype. (a) is a perspective view and (b) shows a projection along the *a*-axis. From Burschka.[12]

literature values of the density are 6.16 g cm^{-3} for PbI_2 and 4.22 g cm^{-3} for $CH_3NH_3PbI_3$.

1.3 Sample preparation and characterisation

The sample preparation aimed for producing perovskite films by sequential deposition, as illustrated in Fig. 3 in the previous section. We decided to use PbI_2 and perovskite films on an underlayer of flat, compact TiO_2 as a model system. The details of PbI_2 deposition and conversion to the perovskite were adapted from the procedure used by Yella *et al.*[10]

Compact TiO_2 underlayer. Prior to deposition of the mesoporous TiO_2 film, the QCM-D sensor or the silicon substrate is cleaned, and an underlayer of thin, compact TiO_2 of approximately 20 nm thickness is deposited. One method applied was atomic layer deposition (ALD) from a tetrakis(dimethylamino)titanium precursor at 150 °C, as described in ref. 18, with subsequent annealing for 3 hours at 420 °C. Alternatively, the underlayer was applied by spray-pyrolysis of an ethanolic solution of di-iso-propoxy titanium-bis(acetylacetone) with an added amount of acetylacetone, using oxygen as a carrier gas for the aerosol,[19–21] and heating the substrate at 420 °C during deposition.

Table 1 Comparison of the crystal lattice parameters of PbI_2 and the tetragonal phase of $CH_3NH_3PbI_3$. Adapted from,[12] based on literature data[13,15,16]

		PbI_2	$CH_3NH_3PbI_3$
Crystal system		Trigonal	Tetragonal
Space group		*P*3*m*1	*I*4/*mcm*
Lattice parameters/Å	*a*	4.558	8.874
	b	4.558	8.874
	c	6.986	12.67
Formula for unit cell volume		$a^2c\ \sin(60°)$	a^2c
Unit cell volume/$Å^3$	*V*	125.7	997.9
Formula units per cell	*Z*	1	4
Volume per formula unit	*V*/*Z*	125.7	249.5
Molecular weight/g mol^{-1}	*M*	461.0	620.0
Density/g cm^{-1}	ρ	6.16	4.22

Deposition of the PbI_2 film. The PbI_2 was dissolved in *N*,*N*-dimethylformamide at a concentration of 600 mg ml^{-1} by heating the solution to 120 °C under occasional stirring. Subsequently, the solution was cooled down to 70 °C. For deposition of an approximately 200 nm thick PbI_2 film on a flat, compact TiO_2 underlayer, 50 μl of solution were applied to the sample by spin-casting at 6000 RPM for 30 s, using an acceleration of 4500 RPM s^{-1}, and by repeating this procedure once. The entire preparation was carried out in a dry-air box.

QCM-D measurement of the conversion and back-conversion. For QCM-D measurements, the sensor with the PbI_2 film was transferred in a closed sample box with dry silica gel from the drybox to the QCM-D setup, where humidity was kept under 5% for most of the time. After mounting the sensor, the flow cell was flushed with pure isopropanol and signal acquisition was re-started soon after the filling of the chamber. After approximately 10 min of rinsing with isopropanol, the liquid handling system was switched to the solution of 8 mg ml^{-1} CH_3NH_3I in isopropanol, which had been prepared previously in a dry box. In order to achieve a rapid exchange of solvent inside the liquid handling system without creating a concentration gradient, the solvent was flushed in at the maximum pump speed for about 30 s. The maximum pump speed is approximately 800 μl min^{-1}. The same procedure was applied when changing back to pure isopropanol. The usual nominal pump speed during the experiment was 100 μl min^{-1}. The experiment in Section 2.2 will show that increasing this regular nominal pump speed to 500 μl min^{-1} does not significantly affect the reaction kinetics in our experiment. We can therefore assume that the kinetics monitored here are not limited by depletion of species from or their accumulation in the solvent.

Humidity control on the QCM-D setup. The technical details of the QCM-D E4 machine and the setup of the flow cell have been explained previously in ref. 22. In order to keep humidity low, but maintain easy access to the liquid handling system, the QCM-D machine was placed in a plexiglas box that was flushed with large currents of dry air and had a large hatch for manipulations. At 35% ambient humidity in the lab, the humidity inside the box was below 5% when the hatch was closed. Upon opening the hatch for manipulation, the humidity would jump up to 20%, but go back down to 5% within 30 s after closing the hatch.

Samples for SEM and XRD. The films for SEM imaging were prepared on Si wafer substrates, that had been coated with a TiO_2 underlayer just as the QCM-D sensors by ALD or by spray-pyrolysis, and the PbI_2 film was deposited in the same way as above unless otherwise mentioned. Sample preparation then continued in a dry air box in analogy to those in the QCM-D experiment: pre-wetting in isopropanol for 10 min, approximately 50 s of immersion in 0.8 μl min^{-1} CH_3NH_3I in isopropanol, and rinsing with isopropanol for 5 min. Different samples were taken out of the process at each stage of interest; *e.g.* after conversion to the perovskite, solvent was removed by spin-coating at 4000 RPM for 30 s and subsequent drying at 70 °C on a hotplate. The samples were stored in dry air for less then 24 hours and transferred to the SEM facility in a closed box filled with dry air and silica gel. After SEM imaging, the same samples were further used for XRD analysis.

2 Reversible interconversion of PbI_2 and MAI to $CH_3NH_3PbI_3$

2.1 Quantitative analysis by QCM-D

A QCM-D measurement of the conversion of PbI_2 and MAI to $CH_3NH_3PbI_3$ perovskite produces a strong and well reproducible signal. Fig. 5 shows experimental data, starting from a 200 nm thick PbI_2 film that is rinsed with plain isopropanol. During the rinse, which corresponds to pre-wetting, a small but continuous up-drift of approximately +40 Hz in 10 min is observed. This is insignificant compared to the overall mass of the PbI_2 film, which corresponds to *ca.* 6600 Hz in frequency shift, and elemental analysis of the outflow suggest that small amounts of iodide are dissolved, but no lead. After $t = 720$ s the film is exposed to 8 mg ml^{-1} CH_3NH_3I in isopropanol, resulting in a stark drop in frequency by −1000 Hz. This is caused by the incorporation of CH_3NH_3I into the PbI_2, resulting in a large mass increase. During the exposure to CH_3NH_3I for more than 60 s, we observe a small linear decrease in frequency, possibly corresponding to a much slower, continued incorporation of CH_3NH_3I. The XRD analysis in Section 2.4 will reveal that we do indeed form the $CH_3NH_3PbI_3$ perovskite, but that about half of the perovskite remains unconverted after 60 s of CH_3NH_3I exposure under these particular conditions. Concomitant to the steep drop in frequency, the dissipation shifts up by 2.0×10^{-5}, correlating with a change in film morphology, as SEM images in Section 2.3 will show. At $t = 800$ s, we start rinsing again with pure isopropanol until the end of the displayed measurement. Almost instantly, the frequency starts to shift upwards in an approximately linear manner until after 180 s, it reaches a plateau at −70 Hz, close to its initial value. The dissipation passes through a maximum of 5.0×10^{-5}, before returning to a value of 1.8×10^{-5}. The linear increase in frequency reflects the dissolution of a species which is identified below by XRD and ICP-MS to be CH_3NH_3I .The peculiar behaviour of the dissipation correlates again with a change in film morphology as

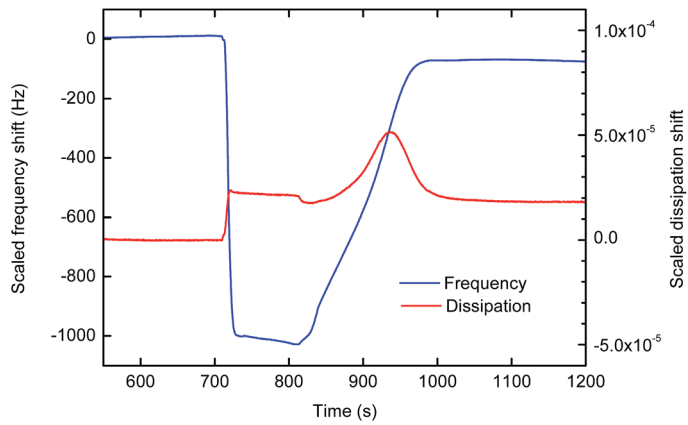

Fig. 5 QCM-D signal of the conversion of a PbI_2 film to $CH_3NH_3PbI_3$ perovskite by exposure to a CH_3NH_3I solution in isopropanol, and the subsequent back-conversion by exposure to isopropanol.

observed by SEM in Section 2.3 and 4. This shift in dissipation will be addressed along with the effect of PbI_2 film morphology on the QCM-D signals in Section 2.5.

The conversion and back-conversion reaction can be repeated several times on the same film, and the PbI_2 itself can be subsequently dissolved in *N*,*N*-dimethylformamide (DMF), as demonstrated in Fig. 6, leading to an increase in frequency of +6600 Hz, keeping isopropanol as a reference. This allows us to estimate the quantity of PbI_2 in the film and compare it to the amount of CH_3NH_3I incorporated during the transformation to the $CH_3NH_3PbI_3$ perovskite.

To estimate the amount of incorporated CH_3NH_3I, we note from the QCM-D measurement in Fig. 5 that the decrease in frequency is approximately −1100 Hz, which corresponds to a change in Sauerbrey mass of $+19.25 \times 10^{-6}$ g cm^{-2}. If we consider that the initial PbI_2 is porous and assume that the $CH_3NH_3PbI_3$ perovskite is not, then we should account for the amount of isopropanol adding to the wet mass of the initial PbI_2 film, which will be discussed in detail in Section 2.5. The amount of trapped isopropanol is 0.97×10^{-6} g cm^{-2}, and the true mass of the incorporated CH_3NH_3I should thus be approximately 20.22×10^{-6} g cm^{-2}. Using the molecular weight of $CH_3NH_3I = 59$ g mol^{-1}, we obtain an amount of 0.127×10^{-6} mol cm^{-2} of incorporated CH_3NH_3I after conversion to the $CH_3NH_3PbI_3$ perovskite for this type of preparation. The dissolution of the back-converted PbI_2 in DMF solvent does result in an increase of frequency by +6600 Hz, which corresponds to a Sauerbrey mass of $+115.50 \times 10^{-6}$ g cm^{-2}. The isopropanol trapped inside the porous, back-converted PbI_2 amounts to an area mass of approximately 4.63×10^{-6} g cm^{-2}, and thus the dry mass of the PbI_2 film should be around 110.87×10^{-6} g cm^{-2}. Assuming that the PbI_2 is stoichiometric, we use the molar mass of $MW_{PbI_2} = 461$ g mol^{-1} and derive the amount of PbI_2 in the film to be 0.240×10^{-6} mol cm^{-2}. The molar ratio between PbI_2 and CH_3NH_3I after conversion to the perovskite is thus approximately (2 : 1) PbI_2 : CH_3NH_3I, and not (1 : 1), as expected for complete conversion. This ratio indicates that only half of the PbI_2 has been transformed to $CH_3NH_3PbI_3$ during the initial exposure to CH_3NH_3I. This finding is in very good agreement with XRD

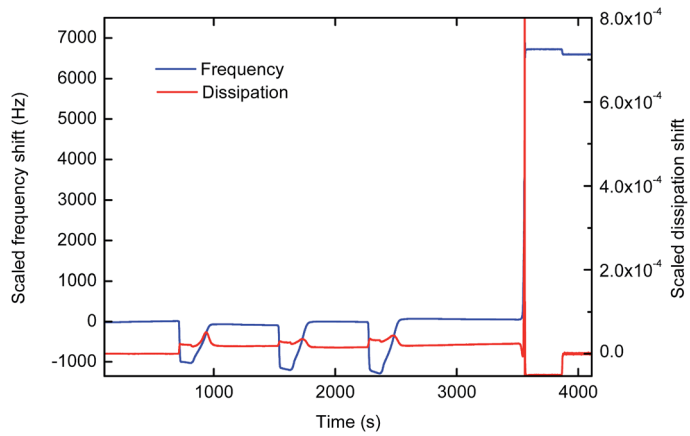

Fig. 6 QCM-D signal of the repetitive conversion of a PbI_2 film to $CH_3NH_3PbI_3$ perovskite, as well as the final dissolution of the PbI_2 in DMF. Subsequent rinsing with isopropanol is in order to account for effects of the bulk liquid on the QCM-D signal.

data presented in Section 2.4. The incomplete conversion on the flat, compact TiO_2 underlayer is in agreement with the general experimental experience, that rapid complete conversion from liquid phase is only achieved for PbI_2 films that are deposited on either mesoporous or very rough compact metal oxides.[6]

We note that the correction made for the liquid trapped inside the pores is smaller than the variation that we observe between different samples made by the same procedure. Initial CH_3NH_3I incorporation produces frequency shifts between −950 Hz and −1200 Hz, and PbI_2 dissolution leads to upshifts between +6000 Hz and +7000 Hz. These variations are probably due to variations in the morphology and thickness of the PbI_2 film, and we have observed occasional irregularities of the dissolution of PbI_2 in the DMF solution prior to spin-casting. We have further observed durations of the back-conversion process that range from 150 s to 250 s. We have carried out the above QCM-D experiment also with flat layers of TiO_2 deposited by ALD or by spray pyrolysis, and we have found no systematic difference in the QCM-D signals for the conversion of the PbI_2 or its re-dissolution.

2.2 Elemental analysis of the outflow by ICP-MS

The QCM-D measurement used for collecting the outflow is shown in Fig. 7. This measurement was performed at a higher nominal pump speed of 500 μl min^{-1} which is five times faster than the usual 100 μl min^{-1}. The increased flow allowed us to avoid intermixing and uncontrolled dilution inside the tubing of the outflow. This was necessary because dissolution processes on the film take place within less than 2 min, and the specific sample had to be taken from the outflow accordingly. Apart from the advantage in technical handling, this measurement shows that the QCM-D results are approximately the same for 100 μl min^{-1} and 500 μl min^{-1} nominal pump speed. Our conversion and back conversion reactions are therefore not limited by depletion or accumulation of chemical species

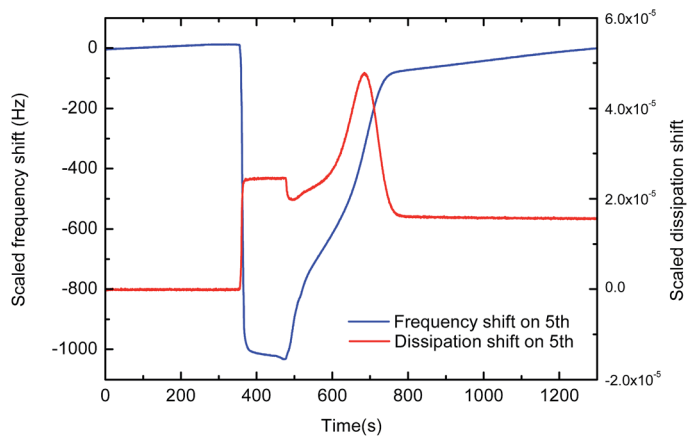

Fig. 7 QCM-D signal of the conversion of a PbI_2 film to $CH_3NH_3PbI_3$ perovskite by exposure to a 10 mg ml^{-1} CH_3NH_3I solution in isopropanol, and the subsequent back-conversion by exposure to isopropanol. The outflow from this measurement was used for elemental analysis by ICP-MS; the nominal pump speed was 500 μl min^{-1}.

in the flow chamber, which might influence reaction kinetics at very low flow speeds. The measurement dates from an earlier period, using 10 mg ml^{-1} CH_3NH_3I in isopropanol.

In Table 2 we present the results of the ICP-MS and the approximate concentrations of lead and iodide in the outflow, collected at a nominal pump speed of 500 μl min^{-1}. The actual ICP-MS measurement was performed on samples diluted with an aqueous solution of 1% nitric acid, in order to obtain measured concentrations in the range of 5 ppb to 500 ppb where precision of the ICP-MS setup is best. The quantitative analysis of lead is very precise (±1 ppb) whereas that of iodide bears a larger error of ±30 ppb.

The outflow during the rinsing of the initial PbI_2 contained small traces of iodide, nominally 670 ppb, but almost no lead was detected (6 ppb). The outflow during exposure to the CH_3NH_3I solution has not been measured due to its excessive iodide content. Upon rinsing of the perovskite with pure isopropanol, the outflow during the significant mass loss, from $t = 850$ s to $t = 1000$ s in Fig. 5, was collected separately from the outflow after the signals had reached a plateau. The solution collected during the mass loss was of a high concentration of iodide, nominally 2.8×10^5 ppb, but only a very small amount of lead (35 ppb). The outflow during the plateau seemed to contain some iodide, nominally 1220 ppb, and very little lead (23 ppb), which is very similar to the outflow from rinsing the initial PbI_2 film.

2.3 Morphology by SEM

The morphology of the films was investigated by scanning electron microscopy acquiring high-resolution images of the top view and of the cross-section. As described in Section 1.4, the films for SEM imaging were prepared on Si wafer substrates, that had been coated with approximately 20 nm TiO_2 by ALD and subsequently annealed for 30 min at 420 °C, so the underlayer was the same as for the QCM-D sensors. The PbI_2 film was prepared the same way as on the on the QCM-D sensors, according to the procedure used by Yella *et al.*[10]

Table 2 Concentrations of lead and iodide in the outflow during conversion and back-conversion obtained by inductive coupling plasma mass spectrometry (ICP-MS). As explained in the text, the concentration of iodide bears a large error, and numbers are understood as nominal values

	Measured concentration on diluted sample		Dilution factor	Estimated concentration in outflow	
	c (I)	*c* (Pb)		*c* (I)	*c* (Pb)
Initial rinsing with isopropanol	67 ppb	0.6 ppb	×10	670 ppb	6 ppb
Mass loss from $t = 500$ s to $t = 750$ s	20 224 ppb	2.5 ppb	×14	2.8×10^5 ppb	35 ppb
Rinsing with isopropanol on the plateau from $t = 850$ s onwards	122 ppb	2.3 ppb	×10	1220 ppb	23 ppb
Final rinsing with DMF	27 ppb	48.5 ppb	>125	—	—

The samples were then prepared in a dry air box in analogy to those in the QCM-D experiment: pre-wetting in isopropanol for 5 min to 10 min, approximately 50 s of immersion in 0.8 mg ml^{-1} CH_3NH_3I in isopropanol, and rinsing with isopropanol for 5 min. Samples were collected at the stage of interest, *e.g.* initially and after conversion to the perovskite. Solvent was removed by spin-coating at 4000 RPM for 30 s and subsequent drying at 70 °C on a hotplate.

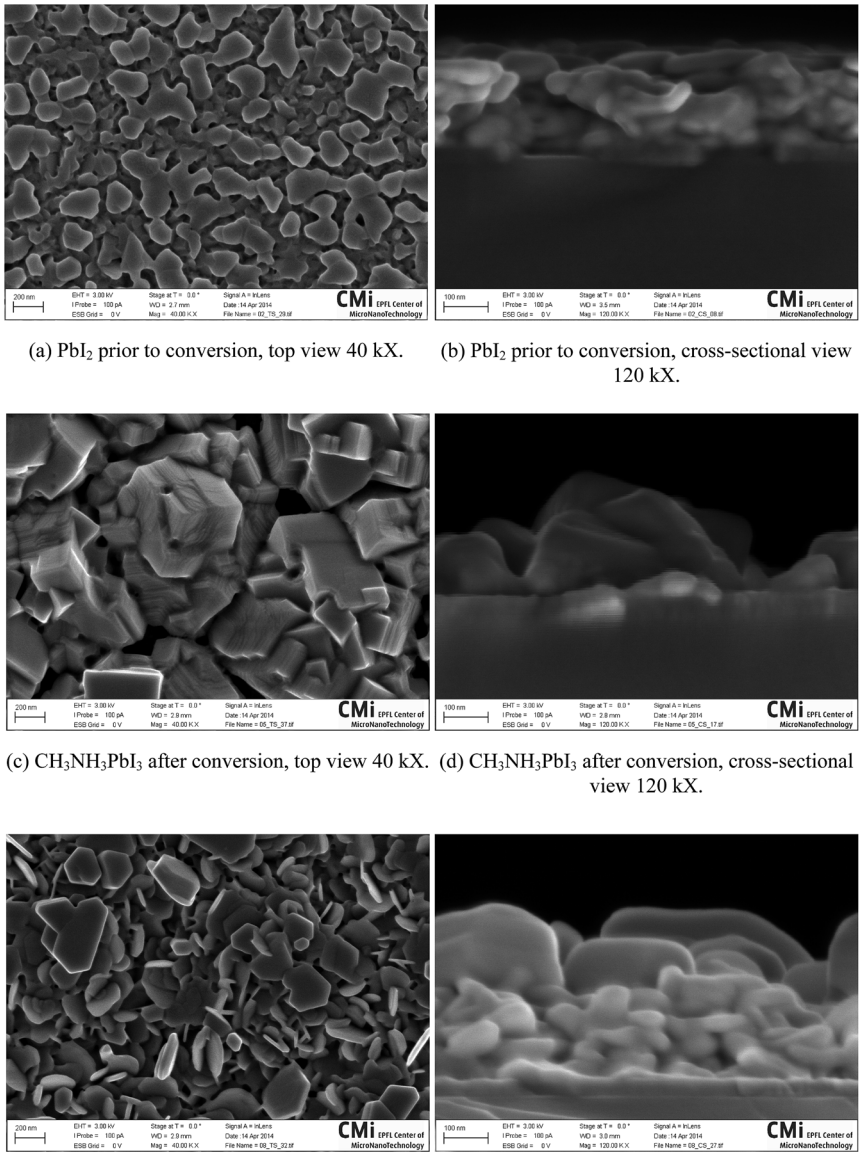

(a) PbI_2 prior to conversion, top view 40 kX. (b) PbI_2 prior to conversion, cross-sectional view 120 kX.

(c) $CH_3NH_3PbI_3$ after conversion, top view 40 kX. (d) $CH_3NH_3PbI_3$ after conversion, cross-sectional view 120 kX.

(e) PbI_2 after back-conversion, top view 40 kX. (f) PbI_2 after back-conversion, cross-sectional view 120 kX.

Fig. 8 SEM images of the film morphology at the major steps of initial, pre-wet PbI_2 (a and b), after conversion to $CH_3NH_3PbI_3$ perovskite by exposure to CH_3NH_3I for 50 s (c and d), and after back-conversion to PbI_2 by rinsing with plain isopropanol for 300 s (e and f).

Fig. 8 shows SEM images of the initial PbI_2 film, after conversion to the $CH_3NH_3PbI_3$ perovskite, and after back-conversion to PbI_2. The top view of the initial PbI_2 film in Fig. 8(a) shows features between 100 nm and 200 nm, and the flat appearance on the top is a result of the double-spin-coating process. The side view in Fig. 8(b) confirms the existence of up to 200 nm large pores, and the locally homogenous film thickness of slightly less than 200 nm. Fig. 8(c) and (d) show the top and cross-sectional view of the film after conversion to the $CH_3NH_3PbI_3$ perovskite by 50 s long immersion in a solution of 0.8 mg ml^{-1} CH_3NH_3I in isopropanol. The SEM images show homogeneously distributed crystallites of cubic appearance, which have lateral dimensions of up to 500 nm and extend to a maximum height of about 300 nm from the surface of the TiO_2 underlayer. Although the cubic crystallites form large protrusions, the film does not show any visible pores. The last set of Fig. 8(e) and (f) show the PbI_2 film after back-conversion from the perovskite by rinsing for more than 5 min with pure isopropanol. The top view (e) reveals a homogenous distribution of up to 200 nm large platelets of hexagonal shape. Most of these platelets have a thickness of approximately 20 nm, though some of them are up to 80 nm thick. The cross-sectional view (f) suggests that the hexagonal platelets lie on top of a layer of smaller particles of a less regular shape. The overall thickness of the layer on this sample is about 350 nm.

The film morphology of the initial PbI_2 and the $CH_3NH_3PbI_3$ perovskite correspond very well to previously published results. Since the back conversion has never been studied explicitly, the PbI_2 film after back-conversion is noteworthy for its pronounced morphology change compared to the initial PbI_2 film. The shape of the particles points to a re-crystallisation process that leads to a larger crystallite size. This is confirmed by XRD in Section 2.4.

2.4 Structural analysis by XRD

The same samples that had been used for SEM imaging in the previous Section 2.3 were subsequently taken for crystallographic analysis by X-ray diffraction (XRD). Fig. 9 shows the spectra of the initial, pre-wet PbI_2, of the film after (partial) conversion to the $CH_3NH_3PbI_3$ perovskite by 50 s exposure to CH_3NH_3I, and of the film after back-conversion to PbI_2 by rinsing with pure isopropanol for more than 5 min. Furthermore, the spectra of a film during back-conversion is shown. In this case, the back-conversion was stopped by starting the drying process of spin-coating and heating after 150 s of rinsing the perovskite film in pure isopropanol.

An overview of the XRD spectra from $2\theta = 10^\circ$ to $2\theta = 60^\circ$ is shown in Fig. 9(a). Fig. 9(b) shows a close-up of the PbI_2-related peak at 12.7° and the $CH_3NH_3PbI_3$ perovskite-related peak at 14.2°, which are exemplary for all PbI_2 and perovskite peaks. The initial PbI_2 peak at 12.7° has an intensity of 640 counts. After conversion to the perovskite, the PbI_2 peak at 12.7° decreases to half of its intensity (360 counts), indicating that only part of the crystalline PbI_2 material has been converted to the $CH_3NH_3PbI_3$ perovskite, which corresponds to the peak at 14.2°. We note that the perovskite peak is actually split into one lower peak at 14.1°, and a second, slightly higher peak at 14.2°. After 120 s of rinsing the perovskite with isopropanol, the back-conversion is not yet complete, as we know from the QCM-D measurements in the beginning of this Section 2.1. However, the according XRD spectrum shows no more perovskite peaks, but a PbI_2 peak at

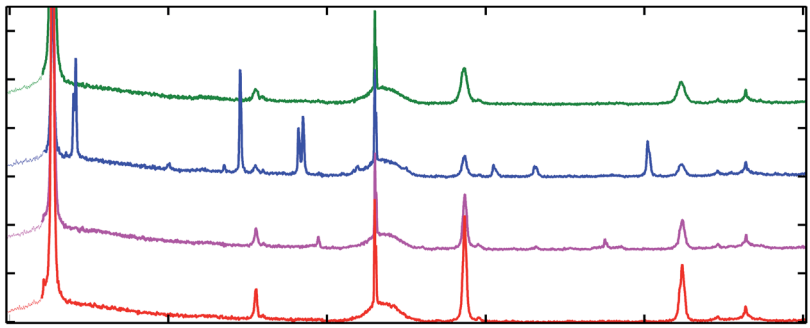

2θ (°)

(a) Complete XRD spectra.

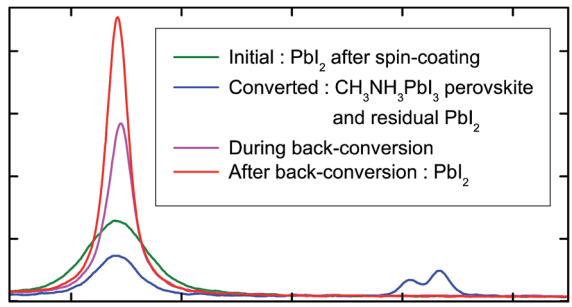

2θ (°)

(b) Details of the PbI_2-related peak at 12.7° and the CH_3NH_3 PbI_3 perovskite peat at 14.2°.

Fig. 9 XRD spectra of the PbI_2 film prior to conversion, after conversion to the $CH_3NH_3PbI_3$ perovskite, during back-conversion, and after completion of the back-conversion to PbI_2.

12.7°, which is of a higher intensity (1420 counts) than the peak of the initial PbI_2. We note that in the complete spectrum in Fig. 9(a), this sample shows two low-intensity peaks at diffraction angles of 29.45° and 47.51°. These two peaks do not exist in any of the other samples in this Figure, and they indicate that the back-conversion may proceed *via* a different crystalline phase. After having rinsed the perovskite for more than 5 min with isopropanol and thus completing the back-conversion to PbI_2, the PbI_2 peak at 12.7° has the highest intensity of all peaks (2270 counts), and the most narrow line width.

This XRD measurement gives important information on the crystal structure, and the different species present. The emergence of the perovskite peak upon CH_3NH_3I exposure, and the decrease of the PbI_2 peak confirm that we have indeed the desired conversion reaction. The fact that the PbI_2 peak does not disappear proves that the conversion is incomplete, though the reaction kinetics have reached a quasi-plateau as seen by earlier QCM-D analysis. Upon back-conversion, the perovskite structure seems to disintegrate before the CH_3NH_3I has

actually left the material. Back-conversion leads to a significant increase in intensity of the PbI_2 peak and to a narrowing of its width, indicating a significant increase in crystallite size upon back-conversion. This correlates very well with the morphology observed by SEM in the previous Section 2.3. We note that the area under the PbI_2 peak is significantly larger after back-conversion than it was on the initial film. Small variations could be related to inconsistent film thickness between the different samples or to the XRD machine. However, the increase in peak area may be an indication that the initial PbI_2 film has a rather amorphous character with a very small average crystallite size, which would result into a much lower peak intensity and area than for larger crystallites.

2.5 Effect of PbI_2 morphology on QCM-D signals

Frequency shift, trapped liquid and effective porosity. Theses measurements aim to understand the influence the morphology of the PbI_2 film on the QCM-D frequency shift and dissipation shift. The porous character leads to a certain amount of liquid trapped inside the film, adding to its wet mass and thereby increasing the measured frequency shift. We furthermore observe an influence of the morphology on the dissipation, indicating a significant drag at the interface between the porous film and the overlying bulk liquid.

We have carried out a QCM-D measurement while changing between two solvents of different density and viscosity, similar to the analysis previously shown on thin mesoporous TiO_2 films.[23] Our choice of solvents was isopropanol ($\rho = 0.781$ g cm^{-3}, $\eta = 2.040$ mPa s) and chlorobenzene ($\rho = 1.106$ g cm^{-3}, $\eta = 0.753$ mPa s), since they do not dissolve PbI_2. The according measurement is shown in Fig. 10: the green line shows the QCM-D response on a flat, compact TiO_2 film as a reference, which corresponds to the changes in bulk viscosity and density of the overlying liquid, and should correspond to the description by Kanazawa and Gordon:[24–26]

$$\Delta f = f_0^{3/2}\sqrt{\frac{\eta\rho}{\pi\mu_q\rho_q}} \text{ and } \Delta D = \frac{1}{t_q\rho_q}\sqrt{\frac{\eta\rho}{\pi f_0}}.$$

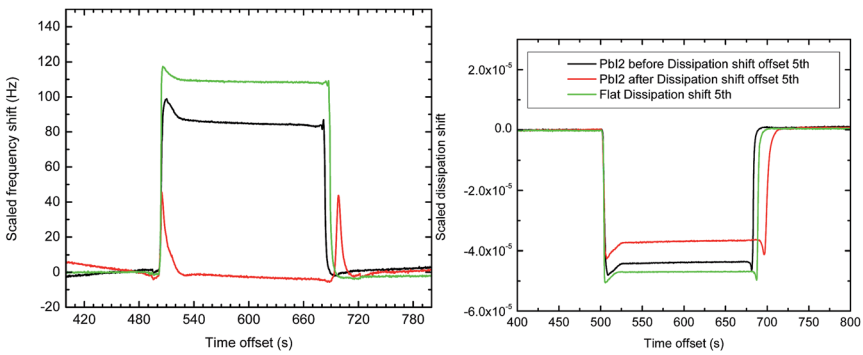

(a) Frequency shift. (b) Dissipation shift.

Fig. 10 QCM-D data for solvent exchange from isopropanol to chlorobenzene and back to isopropanol. Comparing a PbI_2 film prior to conversion (black), the same PbI_2 film after back-conversion (red), and a flat, compact TiO_2 film as a reference (green).

η and ρ are the viscosity and the density of the liquid, and μ_q and t_q are the shear modulus and the transverse sound velocity of the AT-cut quartz. The black line shows the QCM-D response on the initial PbI_2 film deposited by spin-casting prior to conversion. The red line shows QCM-D shifts of frequency and dissipation on the same PbI_2 film after conversion to the $CH_3NH_3PbI_3$ perovskite and back-conversion to PbI_2. The data are offset in time and y-value in order to facilitate a direct comparison.

Table 3 summarises the shifts of frequency and dissipation upon changing from isopropanol to chlorobenzene displayed in Fig. 10 at offset time $t = 560$ s. The last two columns show the differences $\delta f = \Delta f_{PbI_2} - \Delta f_{flat,TiO_2}$ and $\delta D = \Delta D_{PbI_2} - \Delta D_{flat,TiO_2}$ relative to the flat film. We observe a small difference in dissipation shift δD when comparing the dissipation shift on flat film to each of the dissipation shifts on the porous PbI_2. The difference in dissipation shift is $\delta D = +3 \times 10^{-6}$ for the PbI_2 film prior to conversion, and $\delta D = +10 \times 10^{-6}$ for the PbI_2 film after conversion to the $CH_3NH_3PbI_3$ perovskite and back-conversion to PbI_2.

However, for a very rough analysis, we will neglect the shift of dissipation and apply the Sauerbrey equation in order to obtain the approximate amount of trapped liquid from the frequency shift. As a rule of thumb, the Sauerbrey equation is still valid if the dissipation shift in 10^{-6} does not exceed 10% of the value of the frequency shift in Hz. This is the case in the above measurement, and we will discuss the dissipation shift at the end of this section. This rule of thumb, which relates the unit-less dissipation to the frequency shift in Hz, is best understood by recalling that QCM-D measures the properties of a resonance. The frequency shift is the shift of the (central) resonance frequency upon mass loading. The dissipation is proportional to the width of the resonance divided by its absolute frequency, $D = 1/Q = 2\Gamma/f_0 + 3 \times 10^{-6}$, ($D$: dissipation, Q: quality-factor, Γ: full width at half maximum in Hz, f_0: resonance frequency in Hz). The above rule of thumb expresses that the change in the width of the resonance has to be small compared to the shift of the resonance frequency.

The difference in frequency shift δf_{PbI_2} should be primarily related to the change in mass given by the product of the volume of trapped liquid $V_{liq.}$, and the difference in volumetric density ($\rho_{chlorobenzene} - \rho_{isopropanol}$) between chlorobenzene and isopropanol, described by the Sauerbrey equation:

$$-C \times \delta f = \delta m = V_{liq.} \times (\rho_{chlorobenzene} - \rho_{isopropanol}),$$

with the Sauerbrey constant $C = f_0/q_t t_q \approx 17.5$ ng cm^{-2} Hz^{-1}. δm and $V_{liq.}$ are mass and volume per area. Resolving this equation gives the volume of liquid

Table 3 Summarising shifts of frequency and dissipation upon changing from isopropanol to chlorobenzene. Sample surfaces are flat, compact TiO_2, porous initial PbI_2 before conversion, and porous PbI_2 after back-conversion. Values of Δf and ΔD are taken from measurements displayed in Fig. 10 at offset time $t = 560$ s. The last column shows the differences $\delta f = \Delta f_{PbI_2} - \Delta f_{flat,TiO_2}$ and δD relative to the flat film

	$\Delta_{flat\ TiO_2}$	$\Delta_{PbI_2,\ before}$	$\Delta_{PbI_2,\ after}$	$\delta_{PbI_2,\ before}$	$\delta_{PbI_2,\ after}$
Frequency shift Δf, δf in Hz	+109	+89	−1	−23	−110
Dissipation shift ΔD, δD	-47×10^6	-44×10^6	-37×10^6	$+3 \times 10^6$	$+10 \times 10^6$

trapped inside the initial PbI_2 film prior to conversion, and the volume of liquid trapped inside the PbI_2 film after one back-conversion: $V_{liq.}(PbI_2, before) = 1.24 \times 10^{-12}$ m^3 cm^{-2} and $V_{liq.}(PbI_2, after) = 5.92 \times 10^{-12}$ m^3 cm^{-2}.

On the initial PbI_2 film, the trapped isopropanol thus accounts for $V_{liq.}(PbI_2, before) \times \rho_{isopropanol} = 967$ ng cm^{-2} of its wet mass. On the PbI_2 film after back-conversion and before complete dissolution in DMF, the trapped isopropanol accounts for $V_{liq.}(PbI_2, before) \times \rho_{isopropanol} = 4626$ ng cm^{-2} of its wet mass. The latter can be used to calculate the dry mass of the adsorbed PbI_2 by dissolution of the entire film, which gives a measure of its wet mass. We did this in Section 2.1 and obtained a dry area mass of 110.92×10^{-6} g cm^{-2} for the PbI_2 film. Taking into account the density of PbI2, $\rho_{PbI_2} = 6.160$ g cm^{-3}, we can obtain a PbI_2 volume per area of 18.01×10^{-12} m^3 cm^{-2}. For the PbI_2 film after one back-conversion from the perovskite, we measured a trapped liquid volume of 5.92×10^{-12} m^3 cm^{-2}, giving an effective porosity of 24.7%. Prior to conversion, the volume of trapped liquid is approximately 1.24×10^{-12} m^3 cm^{-2}. This leads us to estimate the effective porosity of the initial, spin-cast PbI_2 film to be only around 6.4%.

Dissipation shift and viscoelastic behaviour. Evaluating the difference in dissipation shift observed in the measurement above (Fig. 10) is less straightforward. In order to obtain a general overview, we recall the QCM-D measurement of the conversion from PbI_2 to the perovskite and its back-conversion, as displayed in Fig. 5.

During conversion to the perovskite, the dissipation went up to approximately 25×10^{-6}, including a small contribution from changes in bulk viscosity, which produced 5×10^{-6} dissipation shift on a flat, non-reacting control sample (not shown). During back-conversion, dissipation goes through a peak of approximately 50×10^{-6}, and finally falls back to a value that is 18×10^{-6} higher than on the initial PbI_2 film. Upon dissolution of the PbI_2 film, the dissipation goes approximately back to the same value as the initial PbI_2 film (dissipation shift 0). The SEM picture in Sections 2.3 show, that the change of dissipation clearly correlates with a change in film morphology.

The change in dissipation may be due to a change in the way the surface of the film couples to the overlying bulk liquid. In a simplified picture, the different morphology will produce a different drag in the liquid, which leads to a change in dissipation. This would require to introduce a form factor describing the interface morphology into the equations of Kanazawa and Gordon which describe the coupling to the overlying bulk liquid:

$$\Delta f = f_0^{3/2} \sqrt{\frac{\eta\rho}{\pi\mu_q\rho_q}} \text{ and } \Delta D = \frac{1}{t_q\rho_q} \sqrt{\frac{\eta\rho}{\pi f_0}}.$$

We do not attempt to provide a quantitative description of this correlation yet, but we can try to exclude other possible sources of a shift in dissipation. A common reason for an increase in dissipation would be a softening of the adsorbed film. This is not the case, since the PbI_2 film and the perovskite itself are rigid and they should be well interconnected. It would be possible that the attachment of the PbI_2 film to the TiO_2 underlayer is weakened upon the first conversion and thereby causes an upshift in dissipation. However, we think this is unlikely because the conversion was incomplete in this experiment, and the SEM

pictures in Section 2.3 indicate that some of the PbI_2 close to the TiO_2 substrate does not change its morphology.

Another possible reason for the frequency shift would be turbulent drag due to the flow inside the flow chamber. A turbulent flow can be described by the Reynolds number Re, which is usually defined as a dimensionless number

$$\mathrm{Re} = \frac{\rho v}{\eta}\hat{D}.$$

ρ and η are the density and the viscosity of the liquid, and v is a mean velocity of the liquid. $\hat{D}$ is a form factor of a length unit m, which describes the flow around an object, for example a tube, a sphere, or a rough surface. Below a certain Reynolds number, the flow is laminar, whereas it becomes turbulent above a certain Reynolds number. Increased turbulent flow may lead to increased dissipation in the QCM-D signal as shown by Johannsmann *et al.*[27] However, we do not see any significant change in the dissipation when either stopping the flow, or when pumping with a nominal pump speed of 500 μl instead of the usual 100 μl as shown in Section 2.2, which changes the velocity of the liquid v and thus will influence the turbulent drag.

The quantitative impact of the morphology on QCM-D signals is not understood in detail, and we therefore refrain from further analysis of this phenomena, since its influence on shifts of frequency and dissipation appears to be relatively small compared to the major shifts of frequency due to mass change, which we observe during the conversion and back-conversion reaction.

Concerning the dissipation shift, the most remarkable feature is that during the first conversion, the dissipation shifts up by 20×10^{-6} and then returns approximately to this value after the second and the third cycle of conversion and back-conversion. As explained in Section 2.5, the dissipation shift correlates directly with large changes in film morphology, although we cannot explain the correct mechanism yet. Furthermore, there is an influence of the bulk viscosity and density, which are slightly higher during the exposure to the CH_3NH_3I solution than for the pure isopropanol and account for a shift of approximately $+5 \times 10^{-6}$ on a flat film.

3 Conclusions

Whereas the conversion process from the PbI_2 to the $CH_3NH_3PbI_3$ perovskite has been studied previously by UV-Vis absorption and emission techniques such as XRD and SEM, the back-conversion has not been observed so far. From the data collected until now we can already draw significant insight into this intriguing process. The results presented have been collected on a thin film with an initial PbI_2 thickness of 200 nm but the results should be of general validity, in particular for the mesoscopic systems used in perovskite photovoltaics.

The most evident conclusion from the above results is, that the conversion reaction of PbI_2 to $CH_3NH_3PbI_3$ perovskite is reversible by extraction of the CH_3NH_3I from the perovskite into the solvent. This runs counter to the prevailing contention that the entire perovskite disintegrates in contact with polar solvents.

The implications are numerous. First, the dissolution of the CH_3NH_3I from the perovskite in a moderately polar solvent like isopropanol implies that the same should hold true for any polar solvent, including water. Since CH_3NH_3I is volatile

(the solid sublimes under ambient conditions), this suggests one possible decomposition pathway in humid environments. Strongly polar solvents will equally dissolve parts of the PbI_2.

In general, the reversibility of the conversion reaction should hold true for any lead-halide perovskite, the ease of the transformation being controlled by the interplay of the respective PbX_2 salt and CH_3NH_3X in solution. This also suggests, that a readily formed perovskite of one halide may possibly be converted directly to the perovskite of another halide, simply by exposing to a CH_3NH_3X solution of the second halide. This corresponds to an ion-exchange reaction whose extent is controlled by the mass action law. Importantly we have confirmed recently that a strikingly rapid and facile exchange of halide ions in $CH_3NH_3PbX_3$ can indeed be achieved by solution processing at room temperature [Pellet *et al.*, submitted].

The SEM study in Section 2.3 has shown that the morphology of the PbI_2 film is affected by the conversion and back-conversion, resulting in a PbI_2 film that consists of larger PbI_2 crystallites with improved crystallinity The QCM-D results in Section 3 further indicate that this does increase the amount of incorporated CH_3NH_3I, as well as the size of perovskite crystallites. This effect can be used to direct the morphology in a desired way and improve the overall amount of converted material on flat films.

Beyond the back-conversion, the QCM-D measurements also shed some light on the kinetics of the conversion process from PbI_2 to $CH_3NH_3PbI_3$. There clearly is a rapid initial conversion, which occurs in the first 30 s of the exposure to CH_3NH_3I on a pre-wet sample. This correlates well with optical measurements.[6] However, the QCM-D results suggest that during continued CH_3NH_3I exposure, there is additional CH_3NH_3I incorporated into the film, but at a much slower rate. We recall that the SEM images in Section 3 and 4 indicate that only the upper part of the film is converted to perovskite crystallites, whereas the bottom part resembles the morphology of PbI_2 crystallites. This suggests that the perovskite layer forms a compact cover, impairing the access of CH_3NH_3I to the underlying PbI_2.

References

1 A. Kojima, K. Teshima, Y. Shirai and T. Miyasaka, *J. Am. Chem. Soc.*, 2009, **131**, 6050–6051.
2 J.-H. Im, C.-R. Lee, J.-W. Lee, S.-W. Park and N.-G. Park, *Nanoscale*, 2011, **3**, 4088–4093.
3 H.-S. Kim, C.-R. Lee, J.-H. Im, K.-B. Lee, T. Moehl, A. Marchioro, S.-J. Moon, R. Humphry-Baker, J.-H. Yum, J. E. Moser, M. Grätzel and N.-G. Park, *Sci. Rep.*, 2012, **2**, 1–7.
4 M. M. Lee, J. Teuscher, T. Miyasaka, T. N. Murakami and H. J. Snaith, *Science*, 2012, **338**, 643–647.
5 L. Etgar, P. Gao, Z. Xue and P. Qin, *J. Am. Chem. Soc.*, 2012, **134**, 17396–17399.
6 J. Burschka, N. Pellet, S.-J. Moon, R. Humphry-Baker, P. Gao, M. K. Nazeeruddin and M. Grätzel, *Nature*, 2013, **499**, 316–319.
7 S. Ryu, J. H. Noh, N. J. Jeon, Y. C. Kim, W. S. Yang, J. Seo and S. Il Seok, *Energy Environ. Sci.*, 2014, **7**, 2614–2618.
8 NREL, *Best research-cell efficiencies*, NREL, 2014.
9 H. Mashiyama, Y. Kurihara and T. Azetsu, *J. Korean Phys. Soc.*, 1998, **32**, 156–158.

10 A. Yella, L.-P. Heiniger, P. Gao, M. K. Nazeeruddin and M. Grätzel, *Nano Lett.*, 2014, **14**, 2591–2596.
11 D. Liu and T. L. Kelly, *Nat. Photonics*, 2013, **8**, 133–138.
12 J. Burschka, PhD Thesis, École polytechnique fédérale de Lausanne (EPFL), "High performance solid state mesoscopic solar cells", 2013.
13 T. Baikie, Y. Fang, J. M. Kadro, M. Schreyer, F. Wei, S. G. Mhaisalkar, M. Graetzel and T. J. White, *J. Mater. Chem. A*, 2013, **1**, 5628–5641.
14 Y. Kawamura, H. Mashiyama and K. Hasebe, *J. Phys. Soc. Jpn.*, 2002, **71**, 1694–1697.
15 D. Weber, *Z. Naturforsch., B: J. Chem. Sci.*, 1978, **33**, 1443–1445.
16 S. E. Derenzo, M. J. Weber and M. K. Klintenberg, *Nucl. Instrum. Methods Phys. Res., Sect. A*, 2002, **486**, 214–219.
17 K. Liang, D. B. Mitzi and M. T. Prikas, *Chem. Mater.*, 1998, **10**, 403–411.
18 N. Tétreault, L.-P. Heiniger, M. Stefik, P. L. Labouchère, É. Arsenault, N. K. Nazeeruddin, G. A. Ozin and M. Grätzel, *ECS Trans.*, 2011, **41**, 303–314.
19 F. Matteocci, G. Mincuzzi, F. Giordano, A. Capasso, E. Artuso, C. Barolo, G. Viscardi, T. M. Brown, A. Reale and A. Di Carlo, *Org. Electron.*, 2013, **14**, 1882–1890.
20 L. Kavan and M. Grätzel, *Electrochemistry*, 1995, **40**, 643–652.
21 H. J. Snaith and M. Grätzel, *Adv. Mater.*, 2006, **18**, 1910–1914.
22 H. A. Harms, N. Tétreault, V. Gusak, B. Kasemo and M. Grätzel, *Phys. Chem. Chem. Phys.*, 2012, **14**, 9037–9040.
23 H. Harms, Chapter 4, PhD Thesis,Ecole Polytechnique Fédérale de Lausanne, 2014.
24 K. K. Kanazawa and J. Gordon, *Anal. Chim. Acta*, 1985, **175**, 99–105.
25 K. K. Kanazawa and J. G. Gordon, *Anal. Chem.*, 1985, **57**, 1770–1771.
26 M. Rodahl, *Sens. Actuators, B*, 1996, **37**, 111–116.
27 D. Johannsmann, I. Reviakine and R. P. Richter, *Anal. Chem.*, 2009, **81**, 8167–8176.